Oxidation of tertiary amine derivatised surfaces to control protein adhesion

Dorota A. Dobrzanska,[b,c] Amy L. Cooper,[‡b] Christopher G. Dowson,[c] Stephen D. Evans,[a] David J. Fox,[b] Benjamin R. Johnson,[a] Caroline I. Biggs,[‡b] Rajan K. Randev,[‡b] Helena M. Stec,[b] Paul C. Taylor,[b] Andrew Marsh.[b]*

[a] School of Physics and Astronomy, University of Leeds, Leeds, LS2 9JT, United Kingdom; Tel: +44 113 343 3807; E-mail: s.d.evans@leeds.ac.uk

[b] Department of Chemistry, University of Warwick, Coventry, CV4 7AL, United Kingdom, Fax: +44 24 7652 4112; Tel: +44 24 7652 4565; E-mail: a.marsh@warwick.ac.uk

[c] School of Life Sciences, University of Warwick, Coventry, CV4 7AL, United Kingdom, Tel: +44 24 7652 3534; E-mail: c.g.dowson@warwick.ac.uk

KEYWORDS Self-assembled monolayer, protein resistance, protein adhesion, amphiphile, tertiary amine *N*-oxide, quartz crystal microbalance, AFM, QCM, XPS.

ABSTRACT Selective oxidation of ω-tertiary amine self-assembled thiol monolayers to tertiary amine *N*-oxides is shown to transform the adhesion of model proteins lysozyme and fibrinogen upon them. Efficient preparation of both secondary and tertiary linker amides as judged by X-ray photoelectron spectroscopy (XPS) and water droplet contact angle was achieved with an improved amide bond formation on gold quartz crystal microbalance (QCM) sensors using 2-(1*H*-7-azabenzotriazol-1-yl)-1,1,3,3-tetramethyl hexafluorophosphate methanaminium uronium (HATU). Oxidation with hydrogen peroxide was similarly assessed and adhesion of lysozyme and fibrinogen from phosphate buffered saline then assayed by QCM and imaged by AFM. Tertiary amine functionalised sensors adsorbed multilayers of aggregated lysozyme, whereas tertiary amine *N*-oxides and triethylene glycol terminated monolayers are consistent with small protein aggregates. The surface containing a dimethylamine *N*-oxide headgroup and ethyl secondary amide linker showed the largest difference in adsorption of both proteins. Oxidation of tertiary amine decorated surfaces therefore holds the potential for selective deposition of proteins and cells through masking and other patterning techniques.

1. INTRODUCTION

Surfaces that offer control over the adsorption of proteins[1] and cells[2, 3] find numerous *in vivo*[4-6] and *in vitro* applications, including tissue engineering scaffolds with controlled surface chemistry,[7] selective cell adhesion,[8, 9] and assays in the chemical biology laboratory.[10, 11] Many of these surface chemistries[12-15] also enhance the *in vivo* lifetime and delivery of protein therapeutics.[16] Conversely, bioadhesive surfaces are also prized in nanotechnology, for example in stabilizing enzymes, desirable microbial populations,[17] or even nanotube networks on surfaces

for photovoltaics,[18] and hence chemistries amenable to the discovery[19-22] of both bioadhesive and bioinert surfaces are of great interest.[23] In seeking alternatives to classic poly- or oligoethylene PEG/OEG functionality,[13] we have previously shown[24] that the tertiary amine *N*-oxide moiety, exhibiting kosmotropic properties,[25] is able to enhance resistance to the nonspecific adhesion of a library of genomic polypeptides displayed on the headgroup of phage-λ. Recognising that converting tertiary amines, (which are components of bio-relevant polymers[26, 27] and surfaces[28] finding applications as listed above), to their corresponding *N*-oxides is a straightforward process,[24, 29, 30] we wished to quantify to what extent a protein adhesive surface might be made more resistant to non-specific adhesion. We sought to investigate this using typical test proteins lysozyme[1] and fibrinogen[31] in a quartz crystal microbalance (QCM) assay, to better understand the adsorption process and factors which control it. These new materials will have applications to the patterning of surfaces for protein, cell and nanotube arrays and the discovery of new functional interfacial structures.

Tertiary amine oxide amphiphiles[32] are known to be useful in manipulating and crystallizing membrane proteins,[33] for DNA transfection[34] and are widely used in the household and personal care industry, exhibiting reasonably low toxicity and biodegradability. Whilst often considered to be neutral dipoles,[30] the acid-base behaviour of amphiphilic *N*-oxides is complex[35, 36] and it has been suggested that hydrogen-bonded amphoteric pairs exist at micellar interfaces,[35, 37] particularly when solution p$H \approx$ pK_a of the *N*-oxide.[38] Furthermore, this class of amphiphiles exhibit both concentration and pH dependent pK_a behaviour of the *N*-oxide dipole,[37, 39] hence precise manipulation of interfacial pK_a offers challenges, but promises routes to the selective control of the binding of proteins and cells.

In this article, we demonstrate that a straightforward oxidation step converts protein adhesive tertiary amines to corresponding amine *N*-oxides that display similar resistance to protein adhesion exhibited by triethylene glycol monolayers. We also describe an improved amide bond formation protocol in self-assembled monolayers and explore structure activity relationships for product ω-amines and ω-amine *N*-oxides within these monolayers. The novel surfaces were characterized by X-ray photoelectron spectroscopy (XPS), contact angle measurements, ellipsometry and atomic force microscopy (AFM). Protein – surface interactions were studied by quartz crystal microbalance with dissipation monitoring (QCM-D).

2. EXPERIMENTAL SECTION

2.1. Materials. Reagents (PyBOP®, HATU, isobutyl chloroformate, *N*-methylmorpholine, 30% hydrogen peroxide) were purchased from Aldrich and used as supplied unless otherwise stated. All solvents were purchased from Fisher and were used as supplied unless otherwise stated. Gold-coated QCM sensors were purchased from Biolin Scientific. Lysozyme from chicken white egg and fibrinogen from human plasma were purchased from Sigma-Aldrich (Molecular Biology grade). Glass microscope coverslips were assembled into an Auto306 evaporator and had 2 nm of chromium and ~200 nm of gold deposited at a rate of 0.1–0.2 nm s^{-1}. Coverslips were broken into chips as required and were placed into custom glass vials where they were cleaned in piranha solution at 80 °C for 3 min or placed into the ozone cleaner for 30 min. After cleaning, the chips were rinsed in MilliQ water and then degassed solvent for SAM formation.

2.2. Preparation of gold thiol self-assembled monolayers. Commercial gold-coated QCM sensors, and the gold-coated glass coverslips were cleaned with a piranha mixture (**CAUTION!** Prepare and dispose of small quantities (< 25 mL) only, wear heavy nitrile or butyl rubber gloves and a face mask or additional safety shield and use in an efficient fumehood). Hydrogen peroxide (30%) was added dropwise with stirring to sulfuric acid (98%) 3:1 (v/v), (note the unusual addition of aqueous solution to acid, not *vice versa*) at 80 °C. The samples were immersed in the solution for 3 min to remove organic residues, then rinsed with deionized water and dried in a gentle stream of dry nitrogen. The samples were then immediately immersed in a solution of 16-mercaptohexadecenoic acid in absolute ethanol (1 mM) for 12 hours, then rinsed with absolute ethanol, dried in a gentle stream of dry nitrogen and analyzed by X-ray photoelectron spectroscopy (XPS) without delay.

2.3. Secondary and tertiary amide-linked ω-tertiary amine surfaces. Three methods were used for coupling the amines to 16-mercaptohexadecenoic acid derivatised gold surfaces as follows.

2.3.1. Benzotriazol-1-yl-oxytripyrrolidinophosphonium hexafluorophosphate (PyBOP®) (0.052 mmol, 1 eq) in CH_2Cl_2 (4 mL) was added to each gold-coated quartz sensor in a separate vial. To this vial was added the appropriate amine (0.4 mmol, 10 eq) in CH_2Cl_2 (2 ml) and gently agitated for 24h to produce surfaces **A1**-**A5**. The derivatised sensors were washed with $CH_2Cl_2$and dried in a gentle stream of dry nitrogen before use.

2.3.2. 2-(1*H*-7-Azabenzotriazol-1-yl)-1,1,3,3-tetramethyl hexafluorophosphate methanaminiumuronium (HATU) (0.071 mmol, 1 eq) in CH_2Cl_2 (4 mL) was added to each gold-coated quartz sensor in a separate vial. To this vial was added the appropriate amine (0.4 mmol, 6 eq) in CH_2Cl_2 (2 mL) and gently agitated for 24h to produce surfaces **A1**-**A5**. The derivatised sensors were washed with CH_2Cl_2 and dried in gentle stream of dry nitrogen before use.

2.3.3. Isobutyl chloroformate (0.2 mmol, 1 eq) in dimethylformamide (DMF, 4 mL) was added to each gold-coated quartz sensor in a separate vial in dry DMF (2 mL). To this vial was added *N*-methylmorpholine (0.09 mmol) together with the appropriate amine (0.4 mmol, 2 eq) in dry DMF (2 mL) and gently shaken for 24 h to give surfaces **A1** – **A5**. The derivatised sensors were washed with CH_2Cl_2 and dried in a gentle stream of dry nitrogen before use.

2.4. Tertiary amine *N*-oxides. Surfaces **A1**-**A5** were oxidized with hydrogen peroxide (0.24 mmol of a 30% solution) in ethanol (4 mL) for either 1 h (Leeds) or 12 h (Warwick) and the samples compared by XPS analysis. The sensors were washed with ethanol and dried in a gentle stream of dry nitrogen to give the corresponding amine oxides (**AO1**-**AO5)**.

2.5 Control triethylene glycol surface, **EG**. The control surface bearing 1-aminotriethyleneglycol mercaptohexadecanoic amide (**EG**) was prepared according to the procedure described by Chapman *et al.*[40] The collection of target self-assembled monolayers is shown in Figure 1; see below for discussion.

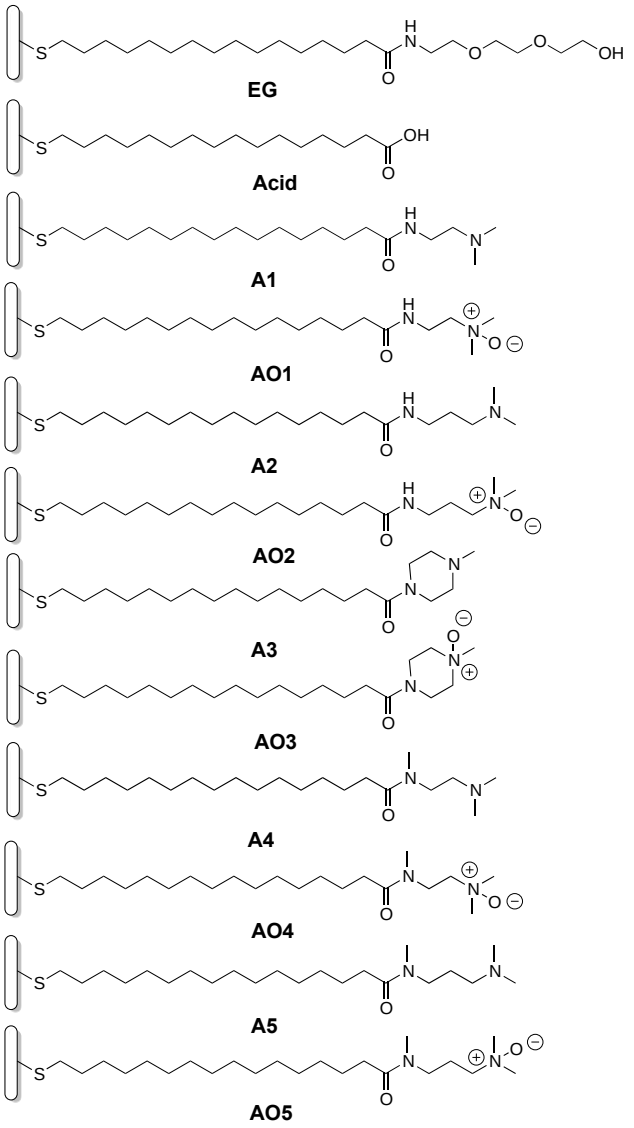

Figure 1 Tertiary amines and tertiary amine *N*-oxide target molecules in this study.

2.5. Ellipsometry (Supporting Information). The average thickness of the surfaces was determined by null ellipsometry (Nanofilm Imaging Spectroscopic Ellipsometer). Measurements yield two angles, Ψ- amplitude ratio and Δ – phase shift. The wavelength scan from 380 nm to 900 nm was performed on three regions of interests at angle of incidence of 70º. The Cauchy equation was used to estimate the monolayer thickness.

2.6. Water contact angle measurements. Static and receding water contact angles were measured on a KRUSS Drop Shape Analyser 100 at room temperature. QCM sensors were washed with ethanol and dried with nitrogen immediately after each measurement. Statistical treatment with the Wilcoxon signed-rank test was used to estimate the validity of the contact angles. This is a nonparametric statistical hypothesis test for the case of two related measurements on a single sample.

2.7. X-ray photoelectron spectroscopy (XPS). XPS measurements were performed using a VG Escalab 250 XPS with monochromated aluminium K-alpha X-ray source. The spot size was 500 μm with a power of 150W. Detailed spectra of individual peaks were taken at an energy of 20 eV. Binding energy was calibrated by setting the carbon 1s peak to 285 eV. Detailed spectra had a Shirley background fitted to them and peaks were data was using mixed Gaussian-Lorentzian fits (using CASAXPS software).

2.8. Quartz crystal microbalance with dissipation monitoring (QCM-D). Protein adsorption was measured using a Q-Sense E4 instrument at 20 °C in at least triplicate and the order of exposure of the surfaces to each protein was measured in both senses in all cases (*i.e.* test surface exposed to lysozyme, cleaned with sodium dodecylsulfate (SDS) then exposed to fibrinogen to acquire a first data set. A freshly prepared surface was then exposed to fibrinogen, cleaned with SDS, and then exposed to lysozyme). No major difference was seen in the protein adsorption kinetics, or amounts of deposition observed between each order of addition. Hence the data presented in Figures 4 and 5 represent the mean of triplicate data with error bars showing standard deviation.

Solutions of phosphate buffered saline (PBS), 5% SDS, fibrinogen (1 μM in PBS) and lysozyme (1 mM in PBS) were prepared and sonicated for 20 minutes prior to the experiment to remove any air from the solutions. The sensors were placed in the chambers and PBS was pumped at a rate of 100 μl/min until the sensors' resonant frequencies equilibrated. The bathing solution was then changed to lysozyme (1 mM) in PBS solution and allowed to equilibrate, whereupon the solution was changed back to PBS to remove any protein resting on the surface. Upon equilibration the solution was finally changed to 5% SDS to more completely clean the surface, followed by a final PBS rinse. At each solution change, the pump was stopped and restarted to avoid any air intake to the system. The sensors were washed with absolute ethanol and dried with nitrogen to remove any remaining proteins. The experiment was repeated with fibrinogen (1 μM) in PBS solution.

2.9 Atomic Force Microscopy. Imaging was carried out in tapping mode at room temperature in air using an Asylum Research MFP-3D atomic force microscope. Three areas of interest on the gold-coated QCM sensors bearing self-assembled ω-tertiary amine monolayers prepared as section 2.3.2 and amine *N*-oxides section 2.4 were selected and imaged in air. The data were treated by MFP3D Igor Pro. Separate sensors were exposed to solutions of lysozyme (1 mM in PBS) and fibrinogen (1 μM in PBS) and after rinsing with PBS and drying under a stream dry nitrogen gas were imaged as above.

3. RESULTS AND DISCUSSION

3.1. Headgroup design and amide bond formation. In previous work[24] we showed that morpholino *N*-oxide headgroups on triazine linkers were similar to triethylene glycol units in resistance to non-specific protein adhesion. We wished to further explore the hypothesis[25] that a reduction in the number of interfacial hydrogen bond donors might further reduce observed protein adhesion, and so designed a small collection of tertiary amines and their *N*-oxides linked through secondary or tertiary amides (Figure 1). We expected the secondary amides to be able to form intermolecular hydrogen bonds to neighbouring molecules, or an intramolecular hydrogen bond between the NH and *N*-oxide moieties.[29] This structural element is absent for the tertiary amides and so together with the larger size of the N-Me(C=O) vs. NH(C=O) group, a more disordered interfacial region should result.

Anticipating straightforward preparation of these materials, we explored the classic 1-ethyl-3-(3-dimethylaminopropyl)carbodiimide (EDC) peptide coupling method both on gold self-assembled monolayers and in solution, but found that the water droplet contact angles and ellipsometric thickness of the amide monolayers was sub-optimal, and in the preparation of analogues in solution (data not shown) a significant impurity co-eluted with the desired product, identified as the *O*-acyl isourea, or rearranged urea of the coupling reagent.[41] Hence on the self-assembled monolayers presented herein we explored alternatives[42] including 2-(1*H*-7-azabenzotriazol-1-yl)-1,1,3,3-tetramethyl hexafluorophosphate methanaminiumuronium (HATU), benzotriazol-1-yl-oxytripyrrolidinophosphonium, hexafluorophosphate (PyBOP®) and isobutyl chloroformate. The efficiency of coupling was estimated from XPS survey scans and high resolution spectra together with water contact angle analysis. Visual inspection of sensor surfaces where coupling was attempted with isobutyl chloroformate revealed a relatively thick

surface layer inconsistent with a self-assembled monolayer, a hypothesis confirmed by a much lower gold peak than expected, hence this method was not considered further.

3.1.1. X-ray photoelectron spectroscopy analysis. Both survey scans and high resolution spectra were carried out for PyBOP® and HATU coupling agents to confirm amide bond formation on the QCM chips. Obvious peaks observed in the survey scan were present at 84-88 eV (Au 4f), 162-164 eV (S 2p), 285 eV (C 1s), 402 (N 1s), 532 eV (O 1s). The high-resolution scans of C 1s show two carbon species: a peak at 289 eV assigned as the carboxylic group and amide peak at 287 eV. This data revealed that HATU gave the clearest nitrogen signal and amide peak indicative of new bond formation. Hence this method was chosen for further work and all the data for surfaces prepared herein arise from HATU coupling.

3.2. Oxidation and characterization. Each surface was then subjected to oxidation using 30% hydrogen peroxide in ethanol and the conversion to tertiary amine *N*-oxide assessed by contact angle, ellipsometry (*vide infra*) and XPS analysis (Supporting Information). In the case of secondary amide **A1** and associated tertiary amide **A4** there was clear evidence of conversion to the *N*-oxides **AO1** and **AO4** shown by a new peak at 403 eV (for example Figure 2). *N*,*N*-Propyldimethylamino surface **AO2** displayed evidence of some *N*-oxidation, but also of loss of material from the monolayer. After treatment with hydrogen peroxide, in the samples examined, neither surfaces **A3** or **A5** exhibited clear peaks at 403 eV attributable to amine *N*-oxide, rather smaller nitrogen and carbon peaks were seen, consistent with significant loss of material in these cases.

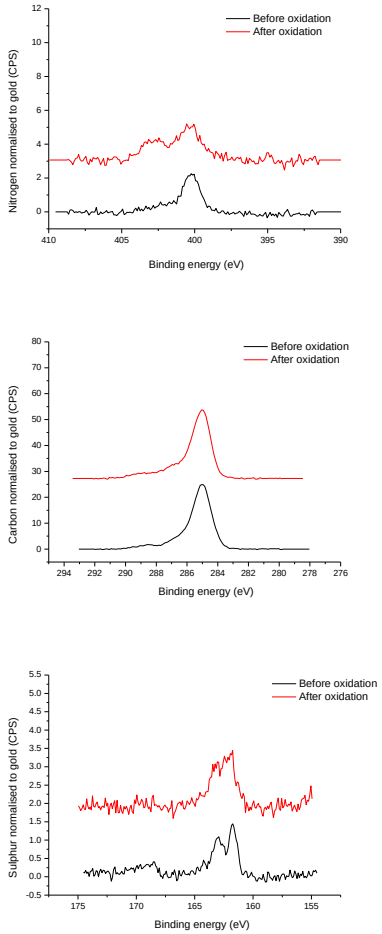

Figure 2 XPS high resolution analysis (*top* to *bottom* N, C, S) of ethyl *N*,*N*-dimethylamino surface **A1** before (red line) and after oxidation, **AO1** (black line) for 12 hours at room temperature.

Surface	Target structure	Average contact angle °	Δ□°	Ellipsometric monolayer thickness (Å)	MMF calc (cos 30°) (Å)
EG	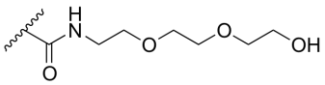	43±2	-	22	23 (gauche)
A1	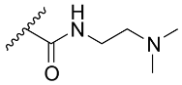	34±3	-	24	24 / 23 cyclic
AO1	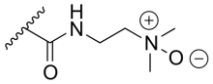	25±2	8	25	24 / 24 cyclic
A2	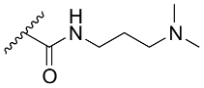	37±6	-	25	26 / 23 cyclic
AO2	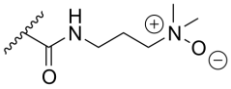	28±4	9	24	26 / 24 cyclic
A3	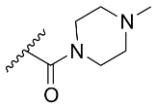	37±4	-	22	24
AO3	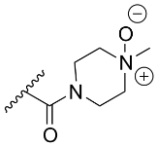	29±3	8	21	23
A4	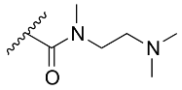	38±2	-	22	25
AO4	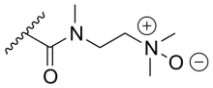	30±2	8	20	24 / 23 cyclic
A5	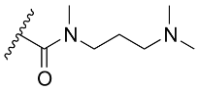	36±3	-	25	25 / 22 cyclic
AO5	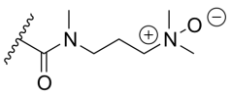	28±2	8	24	24 / 22 cyclic

Table 1 Self-assembled monolayer characterization.

Average contact angle, ± standard deviation (SD) and the difference (Δ) for tertiary amines and corresponding amine oxides produced by 12 h oxidation in ethanolic H_2O_2 representing change in hydrophilicity measured for functionalized QCM sensors. Thickness of self-assembled monolayers as measured by ellipsometry and estimated from a molecular mechanics calculation (molecular mechanics force field, MMF gas phase optimised structure, assuming the alkane chain portion is fully extended. Headgroup conformation is also assumed antiperiplanar or 'cyclic' through formation of a 6 or 7 membered intramolecularly H-bond ring conformation, *vide infra*). The orientation of aliphatic chains of the alkanethiolate was taken to be ~30° with respect to the normal of the gold surface.[43]

Table 1 shows the wetting properties of the monolayers on gold surfaces, thickness estimated by calculation, and measured by ellipsometry. Water wets amine oxides ($\theta(H_2O)$ = 25-30º) better than the corresponding amines ($\theta(H_2O)$ = 33-38º), due to the lower interfacial energy between the film and water ($\gamma_{s/l}$), attributable to the amine *N*-oxide dipole providing an attractive binding site for water molecules. The *N*-methylated tertiary amides **A3** - **A5** did not show a difference in interfacial hydrophobicity compared to the corresponding secondary amides **A1**, **A2**. Confidence intervals place the peroxide treated surfaces **AO2** and **AO3** within the range for their respective precursors, which is in agreement with XPS data for incomplete oxidation. XPS elemental composition (Supporting Information, Table S1) shows a C (1s): Au (4f) ratio for most amines (except **A1**) and amine oxides significantly greater (2.00 – 2.30) than that for the mercaptohexadecanoic acid (1.61) and for that expected from literature values for octadecanethiol (1.8 ± 1).[44] However the largest value in the series of 3.94 arises from the triethylene glycol derivative **EG**. These differences can be attributed in part to attenuation of the gold signal by heteroatoms in the self-assembled monolayer, or impurities and entrained solvent. We note there is no clear correlation of the presence of any impurities seen by XPS with contact angle (Table 1) or protein adhesion measurements (*vide infra*).

3.3. QCM-D measurement of protein adhesion. The degree of protein adhesion to any surface depends upon variables including most importantly, the nature of the protein(s), presence of molecules such as lipids, denaturants or other osmolytes,[45] and temperature. Hence we propose that four measures (i) – (iv) are important when assessing to what extent a surface is resistant to any class of adhering protein (Figure 3).

(i) How much protein becomes adsorbed on the surface (**step 2**); (ii) how much protein is removed after rinsing with buffer solution (**step 3**) hence (iii) the total amount of protein that remains (see Figure 4); and (iv) whether any protein remains after rinsing with a more stringent surfactant, sodium dodecylsulfate (**step 4**). Figure 4 summarises the QCM data for adsorption of lysozyme or fibrinogen (**step 1**) and amount *remaining* after PBS rinse.

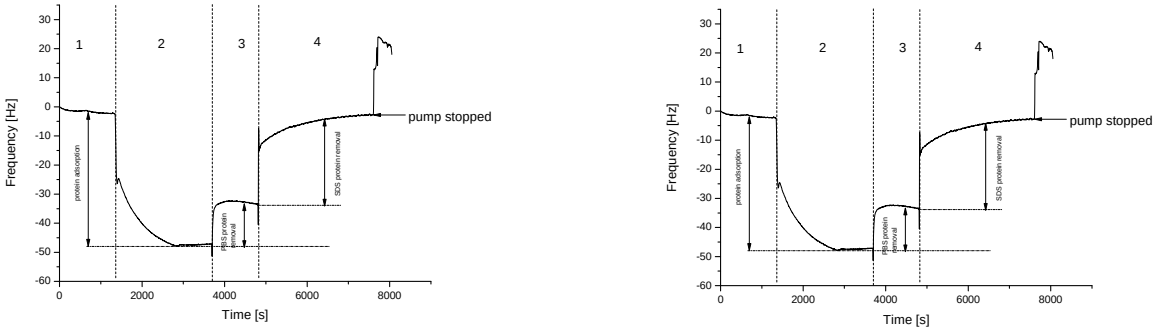

Figure 3 Example data from a QCM-D experiment for lysozyme adsorption (**step 2**) to surface A1 (*left*) and **AO1** (*right*). **Steps 1** and **3** correspond to PBS buffer rinses and **step 4** shows cleaning with sodium dodecylsulfate solution.

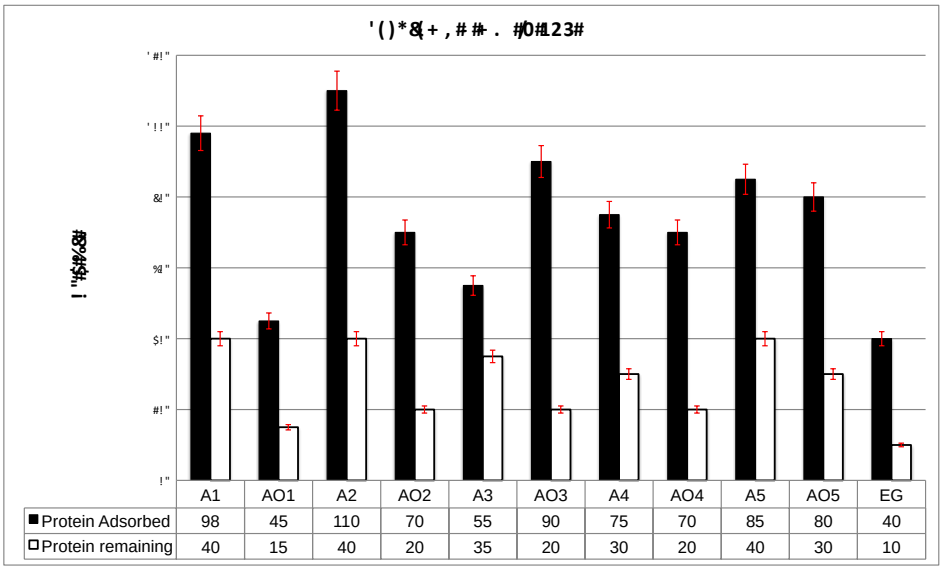

	A1	AO1	A2	AO2	A3	AO3	A4	AO4	A5	AO5	EG
Protein Adsorbed	98	45	110	70	55	90	75	70	85	80	40
Protein remaining	40	15	40	20	35	20	30	20	40	30	10

Chart 1 Adsorption (black) of lysozyme (1 mM) and amount of protein remaining (white) on surfaces after rinsing with PBS buffer. Error bars represent standard deviation of the mean for each surface.

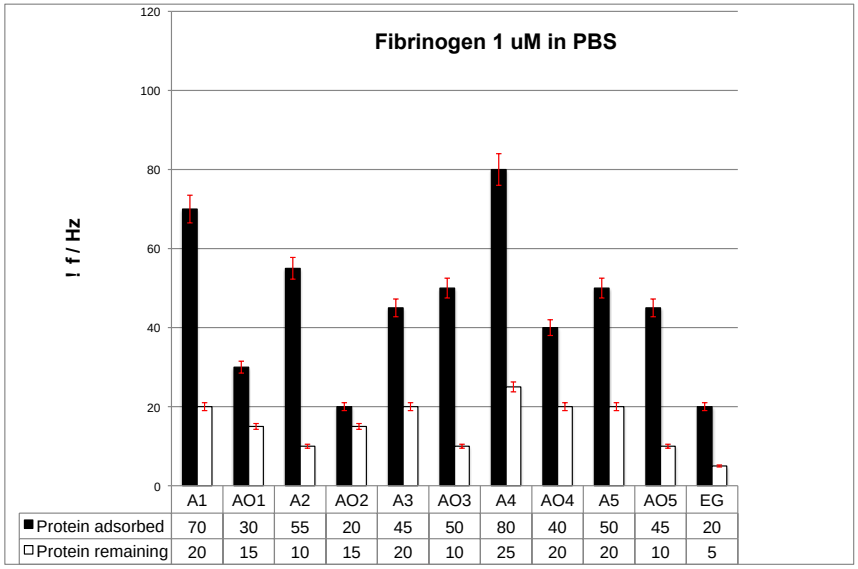

	A1	AO1	A2	AO2	A3	AO3	A4	AO4	A5	AO5	EG
Protein adsorbed	70	30	55	20	45	50	80	40	50	45	20
Protein remaining	20	15	10	15	20	10	25	20	20	10	5

Chart 2 Adsorption (black) of fibrinogen (1 μM) and amount of protein remaining (white) on surfaces after rinsing with PBS buffer. Error bars represent standard deviation of the mean for each surface.

Sample	n	Coverage [ngcm^{-2}] for surface + lysozyme (1 mM PBS)	n	Coverage [ngcm^{-2}] for surface + fibrinogen (1mM PBS)
Bare gold	3	147.5	3	236
A1	3	578	3	413
AO1	3	265.5	3	177
A2	3	649	3	324.5
AO2	3	413	3	118
A3	3	324.5	3	265.5
AO3	3	531	3	295
A4	3	442.5	3	472
AO4	3	413	3	236
A5	3	501.5	3	295
AO5	3	472	3	265.5
EG	3	130	3	218

Table 2 Summary of QCM estimated protein coverage [ngcm^{-2}] for lysozyme (1 mM PBS) and fibrinogen (1 μM PBS) calculated using the Sauerbrey equation: $\Delta m = -C\Delta f n^{-1}$, where C – 17.7 ng Hz^{-1}cm^{-2} for a 5 MHz quartz crystal, Δf – change in frequency (raw data), n – overtone number, n = 3.

The first point to note in comparing data between each protein set (Charts 1 and 2 and Table 2) is that the concentration of fibrinogen (a hydrophobic fibrous protein carrying overall anionic charge, but with key cationic residues implicated in aggregation processes)[46] is one thousand-fold less than lysozyme (a globular protein bearing surface cationic charge at pH 7.4)[47] indicating the nature and concentration[46] of the protein itself has by far the greatest effect on adsorption. Next, with the exception of those surfaces known by XPS to be incompletely oxidized, the biggest differences are seen between amines and their *N*-oxides *e.g.* **A1** and **AO1**.

For example, **A1** with lysozyme adsorbs 578 ng cm^{-2} of protein whereas surface **AO1** adsorbed only 265 ng cm.^{2} of protein. AFM imaging (Figure 4) supports this view, with the amine *N*-oxide surface exhibiting a significantly smoother appearance with what appear to be small clusters of protein (seen in white, Figure 4(d)) after protein deposition, very different in nature from either lysozyme adsorbed on bare gold (control experiment, Figure 4(b)) or on the tertiary

amine (Figure 4(c)). Lysozyme is ellipsoidal in solution with dimension 2.5 x 2.5 x 6 nm,[48] but if the protein partly unfolds,[49, 50] especially in proximity with a surface,[51] aggregates result which although not fibrillar in this case,[52] the assemblies in **A1** (Figure 4(c)) **A2** (Figure 5(c)) and **A3** (Figure 6(c)) are clearly distinct from the spherical clusters on **AO1** (Figure 4(b)), **AO2** (Figure 5(b)) or **AO3** (Figure 6(b)). The image of lysozyme on bare gold is intriguing: despite a relatively low change in QCM-D frequency for either lysozyme or fibrinogen (Table 2), it has striking similarity to that for a nascent multilayer seen in Figures 6(f), 6(g) in the publication by Kim, Blanch and Radke.[51] The smoother appearance of the surface bearing isolated lysozyme clusters on *e.g.* **AO1** (Figure 4(b)) is thus striking, supportive of a mechanism of clustering taking place after deposition, as suggested by those authors. The protein on **AO1** may plausibly be less denatured than that for **A1**, noting that charge-repulsion along the lysozyme polypeptide (expected to be more significant upon a charged amine, rather than neutral amine *N*-oxide surface) has been postulated as central to assembly processes.[53] We have not yet used functional or other assays to explore tertiary structure of the adsorbed enzyme. The surface which adsorbed least lysozyme, **EG** shows much greater similarity to the amine oxides such as **AO1** and **AO2** under AFM imaging (Figure 7).

Surfaces **AO3** and **AO5**, which were observed by XPS to contain less amine *N*-oxide, or have partially lost organic monolayer during the oxidation procedure, show similar levels of protein adsorption to their precursors, confirming the role played by the amine *N*-oxide in the observed differences in protein adhesion.

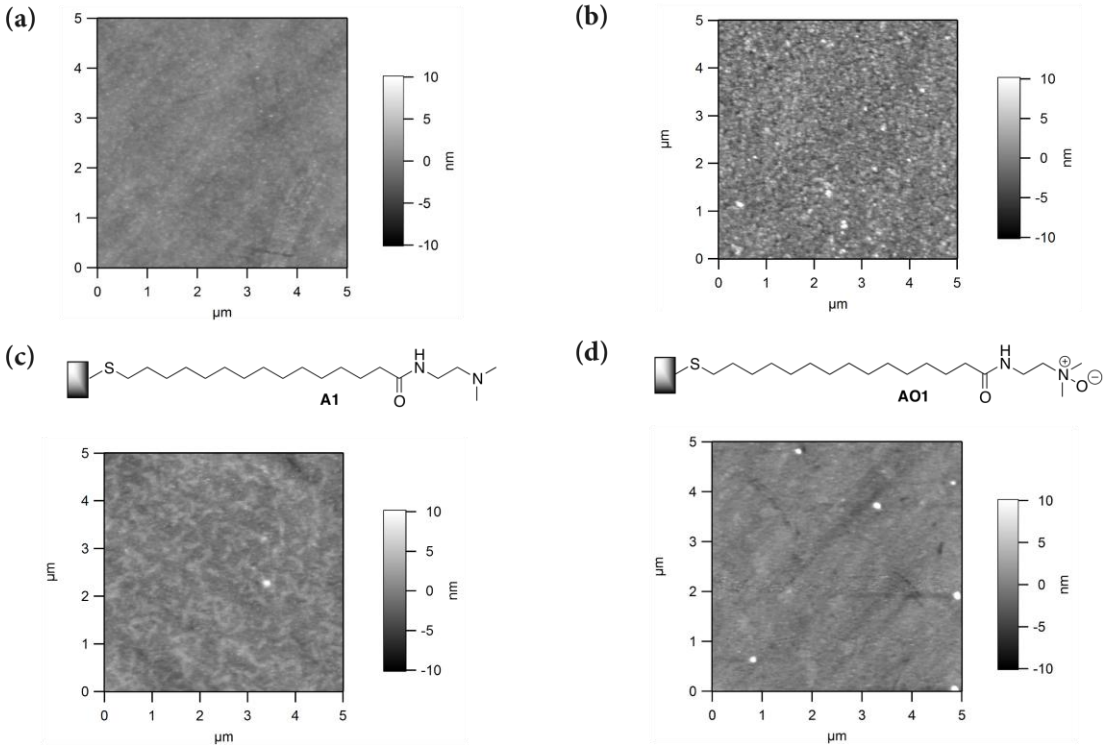

Figure 4 AFM images of: (a) bare gold QCM-D sensor; (b) plus lysozyme, 1 mM in PBS; (c) *N*-[2'-(dimethylamino)ethyl]mercaptohexadecanoic amide plus lysozyme, 1 mM in PBS; (d) *N*-[2'-(dimethylamino-*N*-oxide)ethyl]mercaptohexadecanoic amide self-assembled monolayer plus lysozyme 1 mM in PBS.

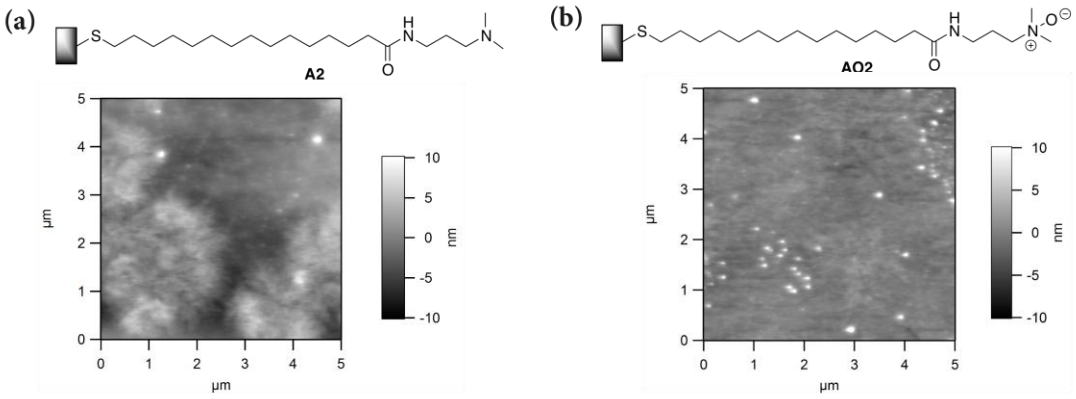

Figure 5 AFM images of: (a) *N*-[2'-(dimethylamino)propyl]mercaptohexadecanoic amide plus lysozyme, 1 mM in PBS; (b) *N*-[2'-(dimethylamino-*N*-oxide)propyl]mercaptohexadecanoic amide self-assembled monolayer plus lysozyme 1 mM in PBS.

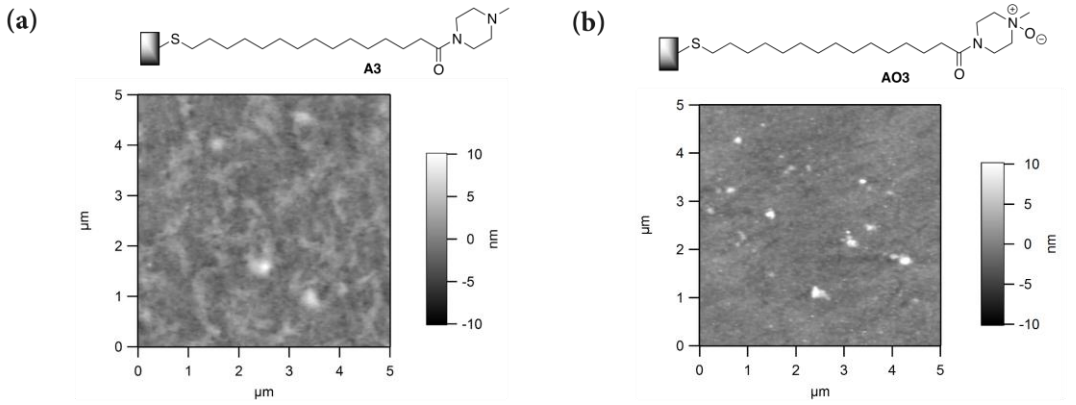

Figure 6 AFM images of: (a) 1-(4'-methylpiperazin-1'-yl-4'-amine)mercaptohexadecanoic amide self-assembled monolayer plus lysozyme, 1 mM in PBS; (b) 1-(4'-methylpiperazin-1'-yl-4'-amine-*N*-oxide)mercaptohexadecanoic amide plus lysozyme, 1 mM in PBS.

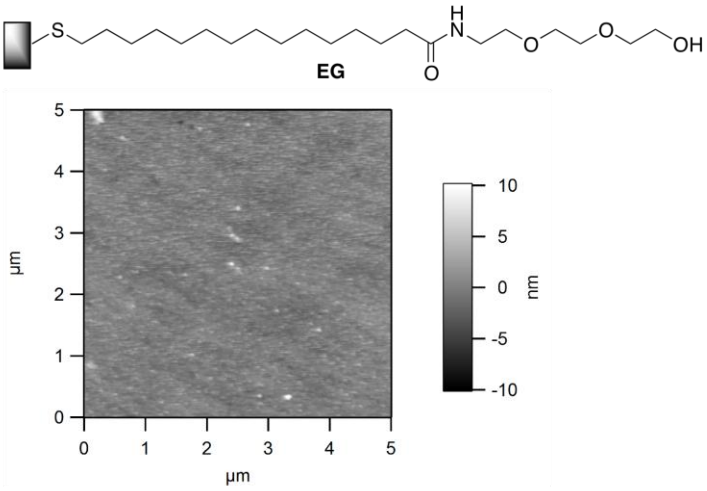

Figure 7 AFM image of 1-aminotriethyleneglycol mercaptohexadecanoic amide self-assembled monolayer plus lysozyme, 1 mM in PBS.

These effects are explicable: (i) through removal of cationic charge carried by the amine surfaces at pH 7.4 and (ii) by the amine *N*-oxide providing dipoles to which water can bind, or that allow the formation of more stable intramolecular hydrogen bonds. The QCM-D data also show (Figure 3 and Supporting Information) that the tertiary amines adsorb both lysozyme and fibrinogen in what appears to be a two-step process leading to multilayers also consistent with significant unfolding of the protein on the more adhesive surface.[50] Fibrinogen (1μM), whose assembly behaviour is known to be concentration dependent, adsorbs to form combined self-assembled monolayer and protein of 25-30 nm thickness on either tertiary amine **A1**, or *N*-oxide **AO1** as measured by AFM. These data are in good agreement with the lower values of Δf recorded by QCM for fibrinogen compared to lysozyme (Chart 2).

The surfaces most resistant to lysozyme adhesion are **EG** and dimethylamine *N*-oxide **AO1**, displaying similar properties for fibrinogen, wherein dimethylamine *N*-oxides **AO1** and **AO2**, are more effective than the established triethylene glycol (Table 2). Direct comparisons of the latter ought strictly to take account of the number of ethylene glycol units. Thus, measured per functional group, tertiary amine *N*-oxide **AO1** is *more* effective than **EG** at resisting adhesion of the two test proteins, indicating that polymeric analogues (*c.f.* Yang et al.[23]) are certainly worth investigating. Whilst hydrated oligoethyleneglycol self-assembled monolayers are known to adopt gauche and helical conformations,[54, 55] the detailed behaviour of amine *N*-oxides such as **AO1-5**, is less well precedented, especially in monolayer form. Amine *N*-oxides are recognized to stabilize cyclic structures when included in peptides, for example as proline *N*-oxide,[29] and TMAO has been shown to preferentially orient its methyl groups away from hydrophobic interfaces, indicating that the methyl groups are relatively polarised.[56] In our work, the headgroup best resisting adsorption of either protein, and removal by PBS washing, **AO1** ought to be able to form an unstrained 6-membered ring between NH and N-O dipole[29] (Figure 8). Intermolecular hydrogen bonding between neighbouring amides remains possible, but repulsive dipolar interactions with the neighbouring amide might also result, adding beneficial disorder to the surface.[57] In comparison, the protonated amine **A1** probably forms a less favored 7-membered ring, leading to a preference for a more regular, extended, rather than gauche conformation in the headgroup.

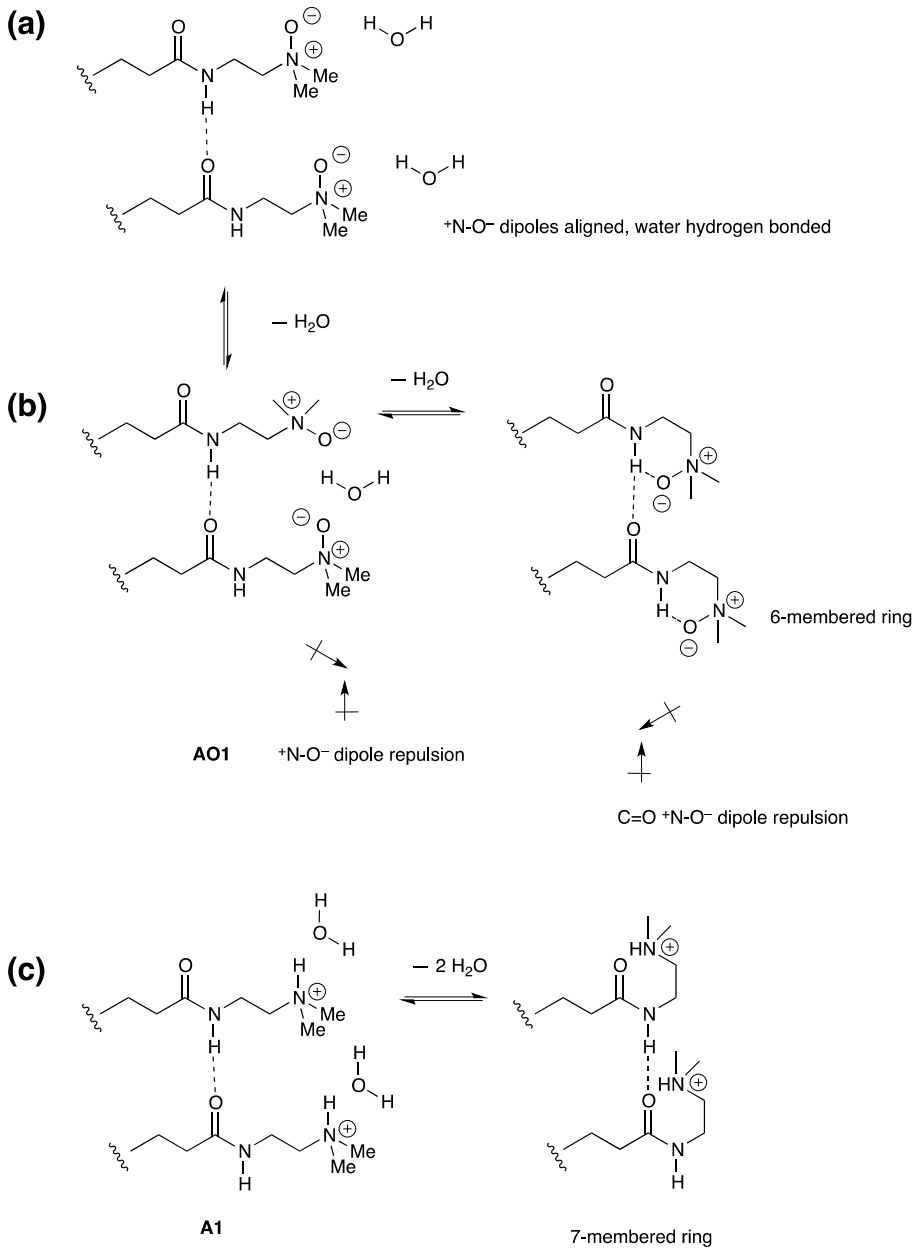

Figure 8 Possible conformations (*a*) and (*b*) for tertiary amine oxide **AO1** (6-membered hydrogen bonded ring)[29] and (*c*) precursor amine **A1** (less favorable 7-membered ring).

Preventing intra- or intermolecular H-bond formation in **AO4** gives a surface that is somewhat more prone to deposition of both positively charged lysozyme and the more hydrophobic fibrinogen, although the ability of both proteins to be removed by PBS rinse remains less

affected. Hence *N*-methylation, or removal of an N–H donor[25] through *N*-methylpiperazine formation, has a significantly smaller effect on protein adsorption behaviour than *N*-oxidation itself. The excellent hydrogen bond acceptor ability of the N-O dipole[58] is therefore sufficient to explain the differences in contact angle, and enhanced protein resistance of amine oxides over the corresponding tertiary amines. There is nonetheless scope for optimization of the oxidation process to ensure that the monolayer integrity is unaffected, or as we show in related work,[59] to use preformed alkylamine *N*-oxides grafted to silicon wafers.

4. SUMMARY AND CONCLUSIONS

We demonstrate a straightforward chemical transformation of protein-adhesive surfaces to tertiary amine *N*-oxides significantly more resistant to the nonspecific adhesion of the model proteins lysozyme (found in physiological fluids such as tears) and fibrinogen (found in blood) at physiological p*H*. The p*H* of the PBS buffer solution was 7.4, so tertiary amines exist largely in their protonated form, whereas amine oxides, with a typical solution pK_a of 4-5[30] might be expected to be unprotonated, although this is recognised to be dependant on aggregation state.[39, 60] Surprisingly, the presence of an *N*-methyl or other tertiary amide function in the linking group was seen to slightly increase adhesion for both classes of protein. We speculate this may be due to the reduction in intermolecular hydrogen bonding, increased barriers to headgroup mobility and larger molecular volumes causing altered surface packing parameters for these analogues. Interestingly, those surfaces did not show increased hydrophobicity as probed by water contact angles. Hence, the optimum features identified from this small set of analogues are that it contains a dimethylamine *N*-oxide headgroup and ethyl (**AO1**) secondary amide linking it to the surface. This provides material with a similar level of resistance to the widely used triethylene

glycol headgroup, with preliminary indications that a less denatured polypeptide has resulted than for the tertiary amines, evidenced by lower quantities seen by AFM imaging.

The treatment of self-assembled monolayers or polymer surfaces[24] containing tertiary amines with mild oxidants, potentially through patterning, is thus a simple way of changing their resistance to non-specific protein adhesion, and diversifying collections of surfaces[20, 21] which contain them. We continue to exploit these observations for the discovery of cell-supporting materials, in particular for methanogenic bacteria for anaerobic digestion processes.

ASSOCIATED CONTENT

Supporting Information.

Ellipsometry, detailed QCM-D traces and AFM depth profile measurements. This material is available free of charge via the Internet at http://pubs.acs.org.

AUTHOR INFORMATION

Corresponding Author

*E-mail: a.marsh@warwick.ac.uk.

‡ Undergraduate Research Project Students (R.K.R. 2005-06, C.I.B. 2009, A.L.C. 2009-10).

The authors declare no competing financial interest.

ACKNOWLEDGEMENTS

We thank the Warwick BBSRC DTC and the Perry Foundation for a Ph.D. studentship and funding to D.A.D. C.I.B. and A.M. thank the Nuffield Foundation for an Undergraduate Research Bursary 2009. H.S. thanks EPSRC for a Ph.D. studentship. We are grateful to Dr Zoe Maple and Stacey Slavin (Department of Chemistry) for assistance with QCM measurements. The QCM-D, ellipsometer and dropshape analyzer used in this research were obtained through Birmingham Science City: Innovative Uses for Advanced Materials in the Modern World with support from Advantage West Midlands (AWM) and part funded by the European Regional Development Fund (ERDF). We thank Professor Tim S. Jones for access to the Atomic Force Microscope and EPSRC for funding this instrument.

REFERENCES

1. Prime, K. L.; Whitesides, G. M., Adsorption of Proteins onto Surfaces Containing End-Attached Oligo(Ethylene Oxide) - a Model System Using Self-Assembled Monolayers. *J. Am. Chem. Soc.* **1993,** 115, (23), 10714-10721.
2. Robertus, J.; Browne, W. R.; Feringa, B. L., Dynamic control over cell adhesive properties using molecular-based surface engineering strategies. *Chem. Soc. Rev.* **2010,** 39, (1), 354-378.
3. Banerjee, I.; Pangule, R. C.; Kane, R. S., Antifouling Coatings: Recent Developments in the Design of Surfaces That Prevent Fouling by Proteins, Bacteria, and Marine Organisms. *Adv. Mater.* **2011,** 23, (6), 690-718.
4. Meyers, S. R.; Grinstaff, M. W., Biocompatible and Bioactive Surface Modifications for Prolonged In Vivo Efficacy. *Chem. Rev.* **2011,** 112, (3), 1615-1632.
5. Szott, L. M.; Horbett, T. A., Protein interactions with surfaces: cellular responses, complement activation, and newer methods. *Curr. Opin. Chem. Biol.* **2011,** 15, (5), 677-682.
6. Li, A.; Luehmann, H. P.; Sun, G.; Samarajeewa, S.; Zou, J.; Zhang, S.; Zhang, F.; Welch, M. J.; Liu, Y.; Wooley, K. L., Synthesis and In Vivo Pharmacokinetic Evaluation of Degradable Shell Cross-Linked Polymer Nanoparticles with Poly(carboxybetaine) versus Poly(ethylene glycol) Surface-Grafted Coatings. *ACS Nano* **2012,** 6, (10), 8970-8982.
7. Grafahrend, D.; Heffels, K.-H.; Beer, M. V.; Gasteier, P.; Moeller, M.; Boehm, G.; Dalton, P. D.; Groll, J., Degradable polyester scaffolds with controlled surface chemistry combining minimal protein adsorption with specific bioactivation. *Nat. Mater.* **2011,** 10, (1), 67-73.
8. Mrksich, M.; Chen, C. S.; Xia, Y. N.; Dike, L. E.; Ingber, D. E.; Whitesides, G. M., Controlling cell attachment on contoured surfaces with self-assembled monolayers of alkanethiolates on gold. *Proc. Natl. Acad. Sci. U. S. A.* **1996,** 93, (20), 10775-10778.
9. Hay, D. C.; Pernagallo, S.; Diaz-Mochon, J. J.; Medine, C. N.; Greenhough, S.; Hannoun, Z.; Schrader, J.; Black, J. R.; Fletcher, J.; Dalgetty, D.; Thompson, A. I.; Newsome, P. N.; Forbes, S. J.; Ross, J. A.; Bradley, M.; Iredale, J. P., Unbiased screening of polymer libraries to define novel substrates for functional hepatocytes with inducible drug metabolism. *Stem Cell Res.* **2011,** 6, (2), 92-102.
10. Jon, S. Y.; Seong, J. H.; Khademhosseini, A.; Tran, T. N. T.; Laibinis, P. E.; Langer, R., Construction of nonbiofouling surfaces by polymeric self-assembled monolayers. *Langmuir* **2003,** 19, (24), 9989-9993.
11. Jonkheijm, P.; Weinrich, D.; Schroder, H.; Niemeyer, C. M.; Waldmann, H., Chemical Strategies for Generating Protein Biochips. *Angew. Chem. Int. Ed. Engl.* **2008,** 47, (50), 9618-9647.
12. Holmlin, R. E.; Chen, X. X.; Chapman, R. G.; Takayama, S.; Whitesides, G. M., Zwitterionic SAMs that resist nonspecific adsorption of protein from aqueous buffer. *Langmuir* **2001,** 17, (9), 2841-2850.
13. Estephan, Z. G.; Schlenoff, P. S.; Schlenoff, J. B., Zwitteration As an Alternative to PEGylation. *Langmuir* **2011,** 27, (11), 6794-6800.
14. Nguyen, A. T.; Baggerman, J.; Paulusse, J. M. J.; Zuilhof, H.; van Rijn, C. J. M., Bioconjugation of Protein-Repellent Zwitterionic Polymer Brushes Grafted from Silicon Nitride. *Langmuir* **2011,** 28, (1), 604-610.

15. Li, Y.; Keefe, A. J.; Giarmarco, M.; Brault, N. D.; Jiang, S., Simple and Robust Approach for Passivating and Functionalizing Surfaces for Use in Complex Media. *Langmuir* **2012,** 28, (25), 9707-9713.
16. Keefe, A. J.; Jiang, S., Poly(zwitterionic)protein conjugates offer increased stability without sacrificing binding affinity or bioactivity. *Nat. Chem.* **2012,** 4, (1), 59-63.
17. Verrier, D.; Mortier, B.; Albagnac, G., Initial Adhesion of Methanogenic Bacteria to Polymers. *Biotechnol. Lett.* **1987,** 9, (10), 735-740.
18. Opatkiewicz, J. P.; LeMieux, M. C.; Bao, Z., Influence of Electrostatic Interactions on Spin-Assembled Single-Walled Carbon Nanotube Networks on Amine-Functionalized Surfaces. *ACS Nano* **2010,** 4, (2), 1167-1177.
19. Pernagallo, S.; Wu, M.; Gallagher, M. P.; Bradley, M., Colonising new frontiers-microarrays reveal biofilm modulating polymers. *J. Mater. Chem.* **2011,** 21, (1), 96-101.
20. Zhou, M. Y.; Liu, H. W.; Venkiteshwaran, A.; Kilduff, J.; Anderson, D. G.; Langer, R.; Belfort, G., High throughput discovery of new fouling-resistant surfaces. *J. Mater. Chem.* **2011,** 21, (3), 693-704.
21. Gu, M. H.; Kilduff, J. E.; Belfort, G., High throughput atmospheric pressure plasma-induced graft polymerization for identifying protein-resistant surfaces. *Biomaterials* **2012,** 33, (5), 1261-1270.
22. Choong, C.; Foord, J. S.; Griffiths, J.-P.; Parker, E. M.; Baiwen, L.; Bora, M.; Moloney, M. G., Post-polymerisation modification of surface chemical functionality and its effect on protein binding. *New J. Chem.* **2012,** 36, (5), 1187-1200.
23. Yang, W.; Xue, H.; Li, W.; Zhang, J. L.; Jiang, S. Y., Pursuing "Zero" Protein Adsorption of Poly(carboxybetaine) from Undiluted Blood Serum and Plasma. *Langmuir* **2009,** 25, (19), 11911-11916.
24. Dilly, S. J.; Beecham, M. P.; Brown, S. P.; Griffin, J. M.; Clark, A. J.; Griffin, C. D.; Marshall, J.; Napier, R. M.; Taylor, P. C.; Marsh, A., Novel tertiary amine oxide surfaces that resist nonspecific protein adsorption. *Langmuir* **2006,** 22, (19), 8144-8150.
25. Kane, R. S.; Deschatelets, P.; Whitesides, G. M., Kosmotropes form the basis of protein-resistant surfaces. *Langmuir* **2003,** 19, (6), 2388-2391.
26. Amalvy, J. I.; Wanless, E. J.; Li, Y.; Michailidou, V.; Armes, S. P.; Duccini, Y., Synthesis and characterization of novel pH-responsive microgels based on tertiary amine methacrylates. *Langmuir* **2004,** 20, (21), 8992-8999.
27. Cerda-Cristerna, B. I.; Cottin, S.; Flebus, L.; Pozos-Guillen, A.; Flores, H.; Heinen, E.; Jolois, O.; Gerard, C.; Maggipinto, G.; Sevrin, C.; Grandfils, C., Poly(2-dimethylamino ethylmethacrylate)-Based Polymers To Camouflage Red Blood Cell Antigens. *Biomacromolecules* **2012,** 13, (4), 1172-1180.
28. Olivier, A.; Meyer, F.; Desbief, S.; Verge, P.; Raquez, J.-M.; Lazzaroni, R.; Damman, P.; Dubois, P., Reversible positioning at submicrometre scale of carbon nanotubes mediated by pH-sensitive poly(amino-methacrylate) patterns. *Chem. Commun.* **2011,** 47, (4), 1163-1165.
29. O'Neil, I. A.; Miller, N. D.; Peake, J.; Barkley, J. V.; Low, C. M. R.; Kalindjian, S. B., The Novel Use of Proline Derived Amine Oxides in Controlling Amide Conformation. *Synlett* **1993,** 1993, (07), 515-518.
30. Bernier, D.; Wefelscheid, U. K.; Woodward, S., Properties, Preparation and Synthetic Uses of Amine N-Oxides. An Update. *Org. Prep. Proced. Int.* **2009,** 41, (3), 173-210.
31. Rodrigues, S. N.; Gonçalves, I. C.; Martins, M. C. L.; Barbosa, M. A.; Ratner, B. D., Fibrinogen adsorption, platelet adhesion and activation on mixed hydroxyl-/methyl-terminated self-assembled monolayers. *Biomaterials* **2006,** 27, (31), 5357-5367.

32. McQuade, D. T.; Quinn, M. A.; Yu, S. M.; Polans, A. S.; Krebs, M. P.; Gellman, S. H., Rigid amphiphiles for membrane protein manipulation. *Angew. Chem. Int. Ed. Engl.* **2000,** 39, (4), 758-761.
33. Rosenbaum, D. M.; Zhang, C.; Lyons, J. A.; Holl, R.; Aragao, D.; Arlow, D. H.; Rasmussen, S. G. F.; Choi, H. J.; DeVree, B. T.; Sunahara, R. K.; Chae, P. S.; Gellman, S. H.; Dror, R. O.; Shaw, D. E.; Weis, W. I.; Caffrey, M.; Gmeiner, P.; Kobilka, B. K., Structure and function of an irreversible agonist-beta(2) adrenoceptor complex. *Nature* **2011,** 469, (7329), 236-240.
34. Goracci, L.; Germani, R.; Savelli, G.; Bassani, D. M., Hoechst 33258 as a pH-sensitive probe to study the interaction of amine oxide surfactants with DNA. *Chembiochem* **2005,** 6, (1), 197-203.
35. Kawasaki, H.; Souda, M.; Tanaka, S.; Nemoto, N.; Karlsson, G.; Almgren, M.; Maeda, H., Reversible vesicle formation by changing pH. *J. Phys. Chem. B* **2002,** 106, (7), 1524-1527.
36. Rathman, J. F.; Christian, S. D., Determination of surfactant activities in micellar solutions of dimethyldodecylamine oxide. *Langmuir* **1990,** 6, (2), 391-395.
37. Kawasaki, H.; Sasaki, A.; Kawashima, T.; Sasaki, S.; Kakehashi, R.; Yamashita, I.; Fukada, K.; Kato, T.; Maeda, H., Protonation-induced structural change of lyotropic liquid crystals in oley- and alkyldimethylamine oxides/water systems. *Langmuir* **2005,** 21, (13), 5731-5737.
38. Kirby, A. J.; Davies, J. E.; Fox, D. J.; Hodgson, D. R. W.; Goeta, A. E.; Lima, M. F.; Priebe, J. P.; Santaballa, J. A.; Nome, F., Ammonia oxide makes up some 20% of an aqueous solution of hydroxylamine. *Chem. Commun.* **2010,** 46, (8), 1302-1304.
39. Goracci, L.; Germani, R.; Rathman, J. F.; Savelli, G., Anomalous behavior of amine oxide surfactants at the air/water interface. *Langmuir* **2007,** 23, (21), 10525-10532.
40. Chapman, R. G.; Ostuni, E.; Yan, L.; Whitesides, G. M., Preparation of mixed self-assembled monolayers (SAMs) that resist adsorption of proteins using the reaction of amines with a SAM that presents interchain carboxylic anhydride groups. *Langmuir* **2000,** 16, (17), 6927-6936.
41. Nakajima, N.; Ikada, Y., Mechanism of Amide Formation by Carbodiimide for Bioconjugation in Aqueous-Media. *Bioconjugate Chem.* **1995,** 6, (1), 123-130.
42. El-Faham, A.; Albericio, F., Peptide Coupling Reagents, More than a Letter Soup. *Chem. Rev.* **2011,** 111, (11), 6557-6602.
43. Nuzzo, R. G.; Dubois, L. H.; Allara, D. L., Fundamental studies of microscopic wetting on organic surfaces. 1. Formation and structural characterization of a self-consistent series of polyfunctional organic monolayers. *J. Am. Chem. Soc.* **1990,** 112, (2), 558-569.
44. Ishida, T.; Tsuneda, S.; Nishida, N.; Hara, M.; Sasabe, H.; Knoll, W., Surface-Conditioning Effect of Gold Substrates on Octadecanethiol Self-Assembled Monolayer Growth. *Langmuir* **1997,** 13, (17), 4638-4643.
45. Evers, F.; Steitz, R.; Tolan, M.; Czeslik, C., Reduced Protein Adsorption by Osmolytes. *Langmuir* **2011,** 27, (11), 6995-7001.
46. Adamczyk, Z.; Bratek-Skicki, A.; Dabrowska, P.; Nattich-Rak, M., Mechanisms of Fibrinogen Adsorption on Latex Particles Determined by Zeta Potential and AFM Measurements. *Langmuir* **2011,** 28, (1), 474-485.
47. Zhang, Y. J.; Cremer, P. S., The inverse and direct Hofmeister series for lysozyme. *Proc. Natl. Acad. Sci. U. S. A.* **2009,** 106, (36), 15249-15253.
48. Krigbaum, W. R.; Kuegler, F. R., Molecular conformation of egg-white lysozyme and bovine alpha-lactalbumin in solution. *Biochemistry* **1970,** 9, (5), 1216-1223.

49. Booth, D. R.; Sunde, M.; Bellotti, V.; Robinson, C. V.; Hutchinson, W. L.; Fraser, P. E.; Hawkins, P. N.; Dobson, C. M.; Radford, S. E.; Blake, C. C. F.; Pepys, M. B., Instability, unfolding and aggregation of human lysozyme variants underlying amyloid fibrillogenesis. *Nature* **1997,** 385, (6619), 787-793.
50. Sethuraman, A.; Vedantham, G.; Imoto, T.; Przybycien, T.; Belfort, G., Protein unfolding at interfaces: Slow dynamics of α-helix to β-sheet transition. *Proteins: Struct., Funct., Bioinf.* **2004,** 56, (4), 669-678.
51. Kim, D. T.; Blanch, H. W.; Radke, C. J., Direct imaging of lysozyme adsorption onto mica by atomic force microscopy. *Langmuir* **2002,** 18, (15), 5841-5850.
52. Chiti, F.; Dobson, C. M., Amyloid formation by globular proteins under native conditions. *Nat. Chem. Biol.* **2009,** 5, (1), 15-22.
53. Hill, S. E.; Miti, T.; Richmond, T.; Muschol, M., Spatial Extent of Charge Repulsion Regulates Assembly Pathways for Lysozyme Amyloid Fibrils. *Plos One* **2011,** 6, (4), e18171.
54. Harder, P.; Grunze, M.; Dahint, R.; Whitesides, G. M.; Laibinis, P. E., Molecular Conformation in Oligo(ethylene glycol)-Terminated Self-Assembled Monolayers on Gold and Silver Surfaces Determines Their Ability To Resist Protein Adsorption. *J. Phys. Chem. B* **1998,** 102, (2), 426-436.
55. Schilp, S.; Rosenhahn, A.; Pettitt, M. E.; Bowen, J.; Callow, M. E.; Callow, J. A.; Grunze, M., Physicochemical Properties of (Ethylene Glycol)-Containing Self-Assembled Monolayers Relevant for Protein and Algal Cell Resistance. *Langmuir* **2009,** 25, (17), 10077-10082.
56. Sagle, L. B.; Cimatu, K.; Litosh, V. A.; Liu, Y.; Flores, S. C.; Chen, X.; Yu, B.; Cremer, P. S., Methyl Groups of Trimethylamine N-Oxide Orient Away from Hydrophobic Interfaces. *J. Am. Chem. Soc.* **2011,** 133, (46), 18707-18712.
57. Herrwerth, S.; Eck, W.; Reinhardt, S.; Grunze, M., Factors that determine the protein resistance of oligoether self-assembled monolayers - Internal hydrophilicity, terminal hydrophilicity, and lateral packing density. *J. Am. Chem. Soc.* **2003,** 125, (31), 9359-9366.
58. Abraham, M. H.; Honcharova, L.; Rocco, S. A.; Acree, W. E., Jr.; De Fina, K. M., The lipophilicity and hydrogen bond strength of pyridine-N-oxides and protonated pyridine-N-oxides. *New J. Chem.* **2011,** 35, (4), 930-936.
59. Dobrzanska, D. A.; Cooper, A. L.; Dowson, C. G.; Evans, S. D.; Haynes, T.; Johnson, B. R.; Stec, H. M.; Taylor, P. C.; Marsh, A., Protein-adhesive and protein-resistant functionalized silicon surfaces. *Langmuir* **2013**, submitted.
60. Kakehashi, R.; Shizuma, M.; Yamamura, S.; Maeda, H., Hydrogen ion titration of alkyldimethylamine oxides by C-13 and H-1 NMR and conventional methods. *J. Colloid Interf. Sci.* **2005,** 289, (2), 498-503.

Table of Contents Only